Physics of Fluids

Elasticity can affect droplet coalescence

Cite as: Phys. Fluids **34**, 093112 (2022); https://doi.org/10.1063/5.0112846
Submitted: 22 July 2022 • Accepted: 25 August 2022 • Accepted Manuscript Online: 27 August 2022 •
Published Online: 21 September 2022

Sarath Chandra Varma, Debayan Dasgupta and Aloke Kumar

Physics of Fluids ARTICLE scitation.org/journal/phf

Elasticity can affect droplet coalescence

Cite as: Phys. Fluids **34**, 093112 (2022); doi: 10.1063/5.0112846
Submitted: 22 July 2022 · Accepted: 25 August 2022 ·
Published Online: 21 September 2022

Sarath Chandra Varma, Debayan Dasgupta, and Aloke Kumar[a)]

AFFILIATIONS

Department of Mechanical Engineering, Indian Institute of Science, Bangalore, Karnataka 560012, India

[a)]Author to whom correspondence should be addressed: alokekumar@iisc.ac.in

ABSTRACT

Coalescence of two droplets on a solid substrate is an interfacial phenomenon that imposes the challenges of capturing the complex contact line motion and energy interaction between the solid–liquid interface. Recent investigations on the coalescence of polymeric droplets on a solid substrate have reported strong disagreements; the heart of the issue is whether coalescence of polymeric drops is similar to that of Newtonian fluid and is independent of molecular relaxation, or whether the role of entanglement of polymeric chains leads to a transition kinetics different from that of Newtonian fluid. Via this article, we resolve the disagreements through a discussion on the effects of merging method on the dominant forces governing the coalescence process, i.e., inertia, dissipation, and relaxation. In this regard, two methods of merging have been identified, namely, the droplet spreading method and the volume filling method. Our study unveils that the coalescence dynamics of polymeric drops is not universal and, in fact, is contingent of the method by which the coalescence is triggered. Additionally, we demonstrate the spatial features of the bridge at different time instants by a similarity analysis. We also theoretically obtain a universal bridge profile by employing the similarity parameter in a modified thin film lubrication equation for polymeric fluids.

I. INTRODUCTION

Coalescence of droplets on a solid surface, also known as sessile–sessile coalescence, is key to a number of commercial applications, including mixing of reagents in microfluidics system,[1] inkjet printing,[2,3] electronic packaging,[4] and rapid prototyping.[5] It involves an initial rapid growth of meniscus bridge, followed by a slow rearrangement of the droplets shape from elliptical to spherical cap at longer times. The presence of solid substrate in such configurations slows down the liquid transport toward the bridge. Once the initial contact is developed between the droplets, the droplet contour is described by the evolution of bridge height, h_b, perpendicular to the substrate and bridge width, r_m, parallel to the substrate. In the case of Newtonian fluids, potential technological interest has driven a lot of effort in investigating the effects of surface wettability,[6–8] surface deformity,[9] viscosity,[10,11] droplet size,[12,13] and contact angle hysteresis[14,15] on the growth of meniscus bridge at both initial and later stages of the coalescence. In particular, Narhe *et al.*[16] proposed a scaling of $h_b \sim t$ and $r_m \sim t^{1/2}$ for initial stages of coalescence, where the capillary number (Ca) was greater than 0.2. Ristenpart *et al.*[17] also reported an exponent of 1/2 for the growth of the meniscus bridge width on a highly wettable surface. A deviation from the proposed scale of $t^{1/2}$ was observed by Lee *et al.*[18] at higher contact angles ranging from 10° to 56°. However, they identified a power law exponent for the bridge height that ranged between 0.5 and 0.86 and increased with increase in contact angle from 10° to 56°. Hernández-Sánchez *et al.*[19] revealed that the bridge height grew linearly with time and evolved with a self-similar dynamics. In addition to the slow viscous regime discussed so far, the bridge height was observed to grow with a universal exponent of 2/3 for contact angle below 90° and an exponent of 1/2 for the contact angle of 90° in the inertial regime.[20–22]

In contrast to Newtonian droplets discussed above, the coalescence of rheologically complex fluids rather remains obscure despite its wide application in droplet 3D printing,[23,24] emulsions,[25–27] and microfluidics.[28] Varma *et al.*[29] highlighted the importance of viscoelasticity viscoelasticty and relaxation time on coalescence of polymeric droplets in a pendant-sessile configuration. A scale of $r \sim t^{0.36}$ was reported for neck growth, which is a significant deviation from $r \sim t$ and $r \sim t^{1/2}$ observed for Newtonian droplets[30–32] in the viscous and inertial regimes, respectively. However, at very high concentrations, Varma *et al.*[33] showed a continuous decrease in power law exponent from 0.36. This is further supported qualitatively by a numerical study on polymers and microgels by Chen *et al.*[34] Even a separate study for coalescence of polymeric droplet in sessile–sessile configuration by Varma *et al.*[35] reported a decrease in exponent from 2/3 in the inertial regime to 1/2 in the viscoelastic regime. Correspondingly, a recent numerical study by Chen *et al.*[36] investigating coalescence of non-elastic, shear-thinning fluid highlighted a strong relation between power law rheology and scaling exponent at the onset of coalescence.

In this regard, it is worth keeping in mind that macromolecular fluids often exhibit strong shear thinning characteristics as well. In contrast, experimental assessment by Dekkar *et al.*[37] highlighted that the presence of polymers causes negligible effect on the temporal evolution of bridge height. This was supported by the observation that a wide range of polymeric concentrations reported a universal power law exponent of 2/3, which is similar to that of de-ionized (DI) water. This lack of consensus regarding the effect of polymer on droplet coalescence is perplexing. In general, the kinematics of coalescence and pinching are not disparate; in fact, Fardin *et al.*[38] revealed the shared and universal features of these flows by showing an excellent collapse of experimental data pertaining to pinching, spreading and coalescence of Newtonian fluids into a universal scale. Interestingly, it is well promulgated that even a minute addition of polymer drastically alters the breakup dynamics of droplets[39,40] by inhibiting pinch off. In this regard, the conclusion by Dekker *et al.*[37] that droplet coalescence is independent of complex fluid rheology seems counterintuitive and demands further exploration.

A closer look reveals that the experimental methods adopted by Varma *et al.*[35] and Dekker *et al.*[37] are different. Varma *et al.*[35] developed the initial contact by creating two pendant droplets of constant volume very close to each other, such that once the drops touched the substrate, they spread to achieve thermodynamic equilibrium. Spreading droplets can create a liquid bridge, as shown in Fig. 1(a). Such coalescence mimics the scenario encountered in ink-jet printed liquid lines and electronic packaging, which require accurate placement of pendant polymeric droplets, so that they spread and merge after impacting the substrate.[41] In the present text, this method is referred to as Droplet Spreading Method (DSM). In a different method as adopted by Dekkar *et al.*,[37] two adjacent droplets are grown simultaneously by increasing the volume until the edges contact and coalescence take place. Such phenomenon is analogous to coalescence due to condensation.[42] This method of merging is referred to as Volume Filling Method (VFM) and is represented in Fig. 1(b). The influence of the two methods of spreading on bridge evolution of Newtonian drops has been demonstrated by Sellier and Trelluyer[43] through numerical modeling and experimental investigation. The neck growth predicted by experiment was observed to be two to three times larger than that of the numerical model. The difference was attributed to the type of merging mechanism; while the merging was due to surface tension induced by capillarity in the numerical simulation, it was induced by volume growth in the experiment. Thus, it can be interpreted that the solid–liquid interface interaction is relatively weaker in VFM as compared to DSM.

Available information in literature shows that the effects of merging process on sessile–sessile coalescence of polymeric drops are yet to be addressed. Typically, the competition among inertia, dissipation, and relaxation leads to the appearance of various coalescence regimes. Our study reveals that a change in the experimental technique may alter the inter-play of the dominant forces and, subsequently, result in an additional regime of coalescence; in essence, the method of triggering the coalescence process can bias the experimental results. In addition, by introducing appropriate scaling parameters, we obtain a representative universal shape of the bridge near the meniscus in the power law regime. Furthermore, we attempt to theoretically demonstrate the universal shape of the bridge by employing the similarity parameter in a modified thin film lubrication equation that describes the effect of polymers at the interface of solid and liquid in the semi-dilute entanglement regime. We believe that the present study will complement the work on coalescence by spontaneous spreading[35] and make the overall research on sessile–sessile coalescence of polymeric drops more complete and comprehensive.

II. MATERIALS AND METHODS

A. Materials

Polyethylene oxide (PEO) of varying concentrations is chosen as the representative polymeric fluid, and the coalescence is carried out on an aluminum substrate. Consistent with Varma *et al.*,[35] we prepare

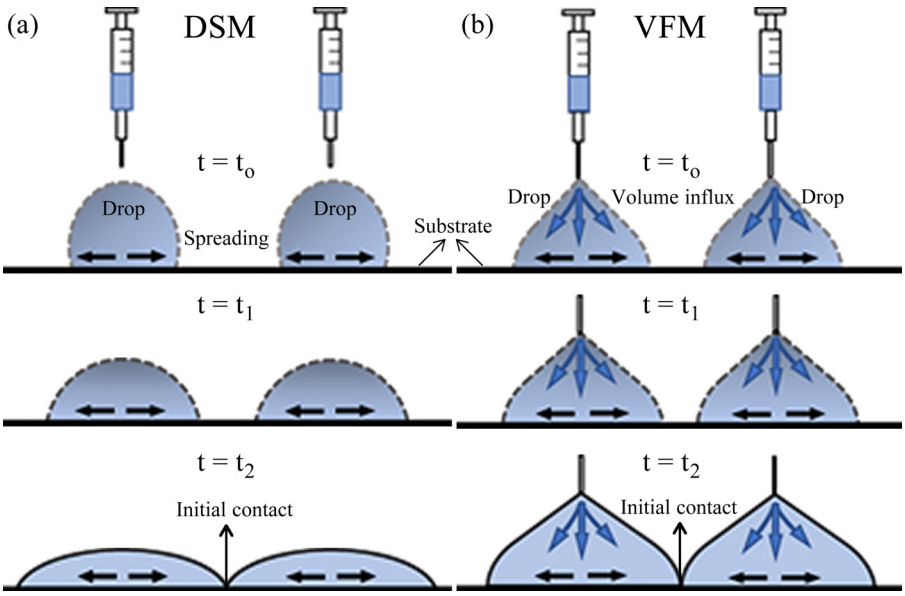

FIG. 1. Merging of two droplets on substrate by (a) depositing fixed volume droplets and allowing them to spread with time $t_o < t_1 < t_2$ to achieve coalescence with an initial contact at $t_o = t_2$ (DSM), (b) continuous pumping of droplets with time $t_o < t_1 < t_2$ till the instance of coalescence at $t_o = t_2$ (VFM). Bold blue arrows represent the fluid influx, while bold black arrows represent the spreading of the droplet.

ten solutions of concentrations c (w/v) 0.01%, 0.02%, 0.05%, 0.061%, 0.1%, 0.2%, 0.3%, 0.4%, 0.5%, and 0.6% by dissolving PEO with molecular weight $M_w = 5 \times 10^6$ g/mol (Sigma-Aldrich) in de-ionized (DI) water. In addition, we prepare another four solutions of sufficiently high concentrations 1.0%, 1.5%, 1.75%, and 2.0% having the same molecular weight. The homogeneity of the solutions is ensured by stirring them at 300 rotations per minute for at least 24 h. The chosen concentrations belong to the dilute ($c/c^* < 1$), semi-dilute unentangled ($1 < c/c^* < c_e/c^*$), and semi-dilute entangled ($c/c^* > c_e/c^*$) regime, where c^* is the critical concentration and c_e is the entanglement concentration.

Measurement of surface tension, σ, by the pendant drop method using optical contact angle measuring and contour analysis systems (OCA25) instruments from Dataphysics yields surface tension values of 0.063 ± 0.02 N/m for all concentration ratios (c/c^*). Density of the solutions obtained by measurement of mass and volume falls in the range of 1000 ± 50 kg/m^3. Hence, a constant density of 1000 kg/m^3 has been assumed for all the polymeric solutions.

To achieve coalescence by VFM, a substrate with higher contact angle is desirable, as it resists spontaneous spreading. Hence, aluminum substrate [RS Components & Controls (India) Ltd.] of dimension $80 \times 30 \times 1.25$ mm^3 is used in the present case, as it displays a high contact angle. Similarly, to achieve coalescence by DSM, a glass substrate (Blue Star, India) of dimensions $75 \times 25 \times 1.45$ mm^3 is used. Substrates are first cleaned with detergent and then sonicated with acetone and water for 20 min each. Subsequently, they are placed in the oven at 95 °C for 30 min. Droplet geometry measured using the ImageJ DropSnake toolbox shows that a contact angle of $72° \pm 3°$ and overall contact length of $2R_0 \approx 3 \pm 0.25$ mm are maintained for all concentrations of PEO solution in VFM.

B. Experimental setup

A fixture having a hollow cylinder with a 45° tilted axis is 3D printed for holding the needles. The needles are inserted through top of the fixture as shown in Fig. 2. Two symmetric drops are grown at the tip of two flat Nordson needles with 0.41 mm inner and 0.71 mm outer diameter. The tip of the needles coming out from the other end is separated by a distance of $l \approx 2$ mm. Initial distance between the needle tip and substrate is kept at 0.55 mm. Once the droplets reach a volume ~3 μl, they touch the substrate. The substrate is further lowered very slowly by a distance of 0.85 mm to ensure that the meniscus connecting the needles to the droplet does not affect the merging process. Finally, coalescence is achieved by quasi-statically advancing the contact lines toward each other due to continuous injection pumping. A small pumping rate of 2 μl/min throughout the process ensures that the droplets are in their equilibrium shape at all time. The liquid supply is stopped as soon as the drops come in contact with each other, and the dispensed volume is noted. Moreover, additional experiments are also conducted for c/c^*=16, 25, 29, and 33 for DSM, following the experimental method of Varma *et al.*[35] A 45 W LED light source (Nila Zaila, USA) at 100% output is used for backlight diffusive illumination of the region of coalescence. A Photron Fast-cam mini AX-100 high speed camera coupled with a Navitar 6.5× zoom lens records the whole process at 60 000 frames per second and 1/100 000 s shutter speed. The shape and evolution of the interface are tracked using a sub-pixel based edge detection algorithm in MATLAB. At first, the images are binarized using an appropriate threshold pixel intensity to get rid of the background disturbances. The coordinate of the column at the contact point of two drops represents the position of the bridge. By tracking the pixel intensities along the column, the row where the pixel intensity falls below the set threshold pixel value is noted. The coordinate values, thus, obtained are utilized to get the surrounding gray intensities in original frame. A pixel weighted average method is implemented to obtain the sub pixel coordinates of the bridge. These coordinates are finally subtracted from the substrate coordinates to obtain the bridge height. The process is repeated for each frame to extract the evolution of the bridge height with time. Similarly, the evolution of the bridge profile $h(x, t)$ in the proximity of h_b is obtained by tracking 15 columns on either side of h_b using the same procedure for each frame.

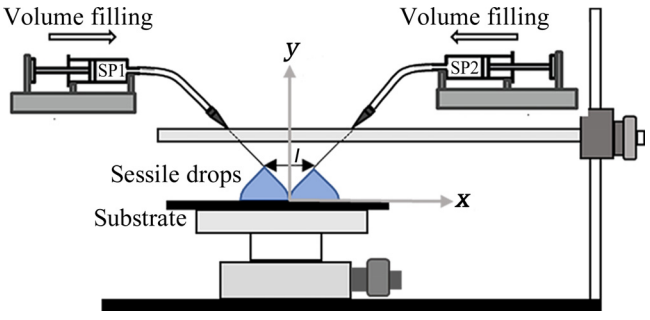

FIG. 2. Schematic of the front view of the experimental setup (SP1 and SP2 are syringe pumps) for VFM, with *l* representing the gap between the needles.

III. RHEOLOGY: CRITICAL CONCENTRATION AND RELAXATION TIME

The critical concentration, c^*, and entanglement concentration, c_e, of the PEO solutions are represented by $c^* = 1/[\eta]$ and $c_e \approx 6c^*$,[44] respectively, where the intrinsic viscosity $[\eta]$ is obtained from Mark–Houwink–Sakurada correlation[45] $[\eta] = 0.072M_w^{0.65}$. For molecular weight $M_w = 5 \times 10^6$ g/mol, a critical concentration value of $c^* = 0.061\%$ (w/v) and entanglement concentration of $c_e = 0.366\%$ (w/v) are, thus, obtained. The relaxation time, λ, in the dilute regime is estimated using the Zimm model,[46]

$$\lambda_z = \Lambda \frac{[\eta] M_w \eta_s}{N_A k_B T}, \tag{1}$$

where λ_z is the Zimm relaxation time, Λ is a pre-factor that depends on solvent quality and is of $\mathcal{O}(1)$, η_s is the solvent viscosity, k_B is the Boltzmann constant, N_A is the Avogadro number, T is the absolute temperature, a is the exponent of Mark–Houwink–Sakurada correlation, and ν is the fractal polymer dimension obtained from $a = 3\nu - 1$. The relaxation time in semi-dilute unentangled and semi-dilute entangled regimes is represented by λ_{SUE} and λ_{SE}, respectively, and is calculated using the correlations $\lambda_{SUE} = \lambda_z \left(\frac{c}{c^*}\right)^{\frac{2-3\nu}{3\nu-1}}$ and $\lambda_{SE} = \lambda_z \left(\frac{c}{c^*}\right)^{\frac{3-3\nu}{3\nu-1}}$,[47–49] respectively. The relaxation times and concentration ratios, c/c^*, corresponding to the chosen concentrations in the study are listed in Table I. Zero shear viscosity, η_o, of the solutions given in Table I is obtained from Varma *et al.*[35] for $c \leq 0.6\%$ (w/v) and from Varma *et al.*[33] for $c > 0.6\%$ (w/v). For completeness, the

TABLE I. Rheological properties of the solutions.

c (%w/v)	Concentration ratio (c/c^*)	η_o (mPa s)	λ (ms)
0	...	1	DI water
0.01	0.16	1.3	1.5
0.02	0.32	1.5	1.5
0.05	0.82	2	1.5
0.061	1	3	1.5
0.1	1.6	6	2
0.2	3.9	18	2.7
0.3	5	46	3.5
0.4	6.5	60	74
0.5	8.2	200	115
0.6	9.8	500	160
1.0	16	4.5	500
1.5	25	20	670
1.75	29	40	1325
2.0	33	55	1350

variation of viscosity, η, with a shear rate, $\dot{\gamma}$, for all the concentrations, is shown in Fig. S3.

IV. RESULTS AND DISCUSSION

The initial contact between droplets is obtained by quasi-statically increasing the droplet volumes at a pumping rate of 2 μl/min. At the beginning of the coalescence, a tiny liquid bridge develops at the point of contact between the droplets. The large curvature of the bridge results in fluid flow from the close neighborhood toward the bridge region due to capillary action. This fluid flux may disturb the equilibrium at the pinned ends at intermediate stage of coalescence when the bridge relaxes, causing a change in contact angle. However, the time taken for the disturbance to reach the pinned end is much higher than the time scale of interest for the present case. Hence, the contact angle is considered to be constant for all practical purposes.

Figure 3(a) shows the schematic of the drop coalescence, where $2R_0 \approx 3 \pm 0.25$ mm represents the contact length and $\theta \approx 72^\circ \pm 3^\circ$ represents the contact angle. Evolution of the liquid bridge during the coalescence of two PEO droplets with concentration ratio $c/c^* = 8.2$ obtained by VFM and DSM is shown in Figs. 3(b) (Multimedia view) and 3(c), respectively, at different instants of time.

Figures 4(a) and 4(b) show the temporal evolution of the bridge height $h_b = h(0, t)$ obtained by VFM and DSM, respectively, for the complete range of c/c^*. The bridge height values are the average of five trials conducted for each solution. The experiments are extremely repeatable, and the error in measurement is limited to $\pm 5\%$. The region of interest (ROI) is considered in such a way that it corresponds to the linear portion of the initial neck growth. As can be seen in Figs. 4(a) and 4(b), a slight shift in the ROI toward left or right for $c/c^* \leq 9.8$ will not affect the power law exponent. However, to make it consistent across various concentration ratios, we have fixed the ROI as shown in Figs. 4(a) and 4(b). For $c/c^* > 9.8$ in Fig. 4(a), there exists more than one power law behavior, but our study focuses only on the initial regime. It can be observed that the regions of interest (ROI) corresponding to the early power law regime is at relatively smaller times

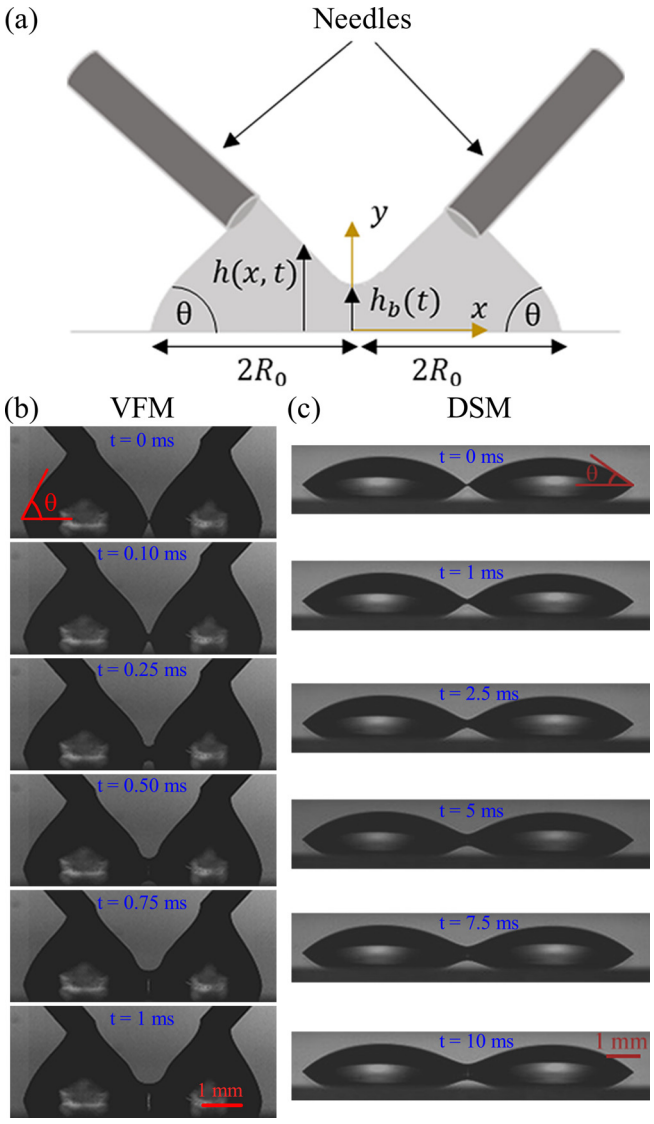

FIG. 3. (a) Schematic of the coalescence representing the geometric parameters and contact angle θ for VFM. Snapshots showing the bridge evolution of 0.5% (w/v) concentration ($c/c^* = 8.2$) of PEO at different instants of time by (b) VFM and (c) DSM. Multimedia view: https://doi.org/10.1063/5.0112846.1

scales for VFM as compared to DSM for the same polymer concentration ratios. In the case of VFM, Fig. 4(a) shows that the exponent b of the power law growth registers a constant value of 2/3 for $c/c^* \leq 9.8$, beyond which it continuously reduces with increase in c/c^*. For the considered range of c/c^*, b does not seem to achieve any stable value. On the other hand, when coalescence is triggered by droplet spreading [Fig. 4(b)], the presence of polymer clearly affects the growth of the meniscus bridge even at small polymer concentrations ($c/c^* < 1$). This is highlighted by a reduction in the exponent of growth from 2/3 for $c/c^* < 1$ to a constant value of 1/2 for $c/c^* > 1$. Correspondingly, the exponent b deduced by fitting the power law curve $h_b \sim t^b$ is shown in Figs. 4(c) and 4(d) for VFM and DSM, respectively. A larger

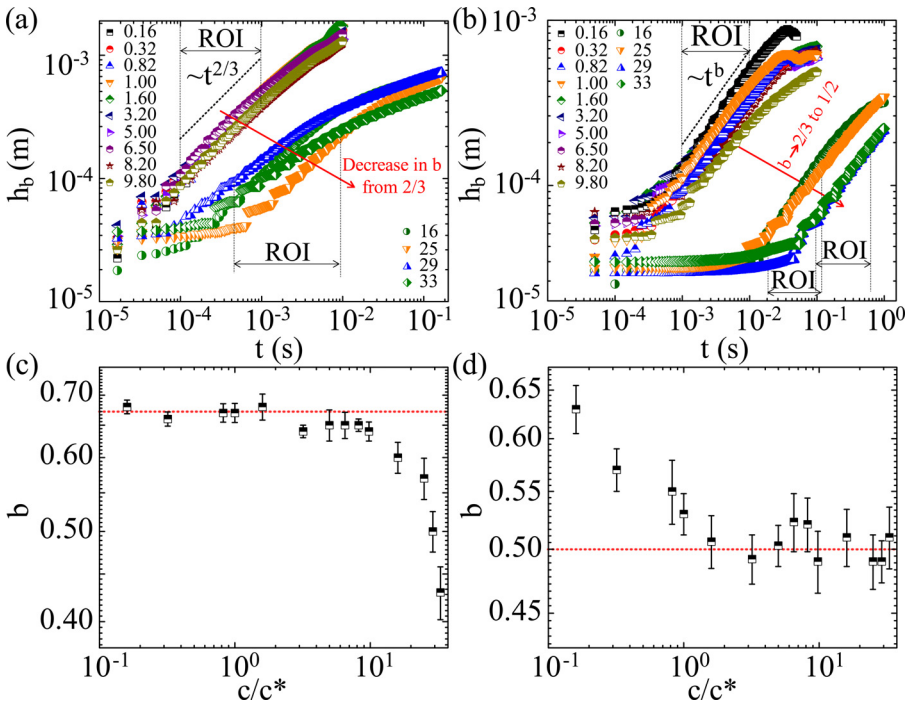

FIG. 4. (a) Temporal evolution of bridge height by VFM showing a constant power law exponent b of 2/3 for $c/c^* \leq 9.8$ and monotonous reduction with c/c^* for $c/c^* > 9.8$. (b) Temporal evolution of bridge height by DSM obtained from Varma *et al.*[35] along with experimentally obtained data for four additional concentrations ($c/c^* = 16$, 25, 29, and 33) showing a decrease in exponent b from 2/3 to 1/2 with increase in c/c^*. (c) Variation of exponent b with c/c^* for VFM. (d) Variation of exponent b with c/c^* for DSM.

power law exponent necessarily implies a faster coalescence process. As a result, it can be said that VFM leads to a faster coalescence as compared to DSM until the exponents become equal at $c/c^* \approx 25$. Beyond $c/c^* \approx 25$, a further drop in exponent is seen for VFM with increase c/c^*, implicating that the process eventually become slower than DSM. The apparent contrast in the flow kinetics for the two methods suggests that the effect of polymers on coalescence is strongly influenced by the experimental method. A qualitative discussion on the behavior of polymer chains subjected to the two methods throws some light on the associated disparity. When the droplets are maneuvered toward each other by spontaneous spreading through DSM, the polymeric chains get elongated along the solid–liquid interface due to the induced shear rate and attain an unrelaxed state. As polymeric concentration increases, these unrelaxed polymer chains offer stronger resistance to the growth of the bridge in the normal direction to solid–liquid interface, which results in a decrease in the growth exponent, as observed in the case of Varma *et al.*[35] However, in the present case of VFM, where the droplets approach each other due to continuous influx of liquid by pumping, the polymeric chains do not undergo enough elongation and mostly remain relaxed. Subsequently, the resistance offered by the polymeric chains to the initial bridge growth is relatively weak. Moreover, the effect of inertial forces induced by continuous pumping in VFM also needs to be considered. Notably, Dekker *et al.*[37] also observed a continuous reduction in exponent b with c/c^* at higher values of c/c^* but contributed the same to error arising from determining the initial point of coalescence. However, in addition to the qualitative explanation provided above, we address this phenomenon by identifying the dominance of the underlying forces through two time averaged non-dimensional numbers—Reynolds number, $Re = \langle \rho u_c l_c/\eta_o \rangle$, and the Weissenberg number, $Wi = \langle \lambda u_c/l_c \rangle$, where η_o is the zero shear viscosity, $u_c \sim \partial h_b/\partial t$ is the characteristic velocity scale, and $l_c \sim h_b$ is the characteristic length scale. We wish to point out that here Re and Wi are only evaluated within ROI window and not across the experimental time domain. Here, $u_c l_c$ in Re and u_c/l_c in Wi have a weak dependence on time. This suggests that the $\mathcal{O}(Re)$ and $\mathcal{O}(Wi)$ remain almost same in the ROI. Hence, the time averaged Re and Wi can be considered to be a fair representation of the instantaneous Re and Wi.

Figures 5(a) and 5(b) show a comparison between Re and Wi values obtained by the present VFM method and that obtained via DSM by Varma *et al.*,[35] respectively. In the subsequent discussion, the inertial, viscous, and elastic forces are represented by F_i, F_v, and F_e, respectively. At first, we consider the influence of c/c^* on Re and Wi for VFM. It can be observed that $Re \sim O(10^2)$ and $Wi \sim O(10^0)$ for $c/c^* < 1.6$. Hence, the sequence of the participating forces is described as $F_i \gg F_v \sim F_e$, and the corresponding regime is identified as an inertia dominated regime (ID). For $1.6 < c/c^* < c_e/c^*$, Re ranges between $O(10^1)$ and $O(10^0)$, and Wi approaches $O(10^1)$, thereby representing an inertio-elastic regime (IE), where $F_e \sim F_i > F_v$. In the subsequent region $c_e/c^* < c/c^* < 10$, a viscoelastic regime (VE) is identified, where $Re \sim O(10^{-1})$ and $Wi \sim O(10^2)$, such that $F_e > F_v > F_i$. At sufficiently high polymer concentrations $c/c^* > 10$, Re approaches $O(10^{-5})$ and Wi approaches $O(10^3)$, which suggests that both the inertial and viscous forces become negligible, and the flow dynamics is completely taken over by the elastic forces. This results in an elasticity dominated regime (ED) characterized by $F_e \gg F_v \gg F_i$. A similar comparison between Re and Wi values for DSM in Fig. 5(b) reveals three regimes, namely, inertio-elastic, visco-elastic, and elasticity dominated regimes. A regime-wise comparison between the two methods reveals that the inertial forces are more prominent in the case of VFM, as compared to DSM. In fact, no inertia dominated regime is observed for DSM. At most, the inertial forces

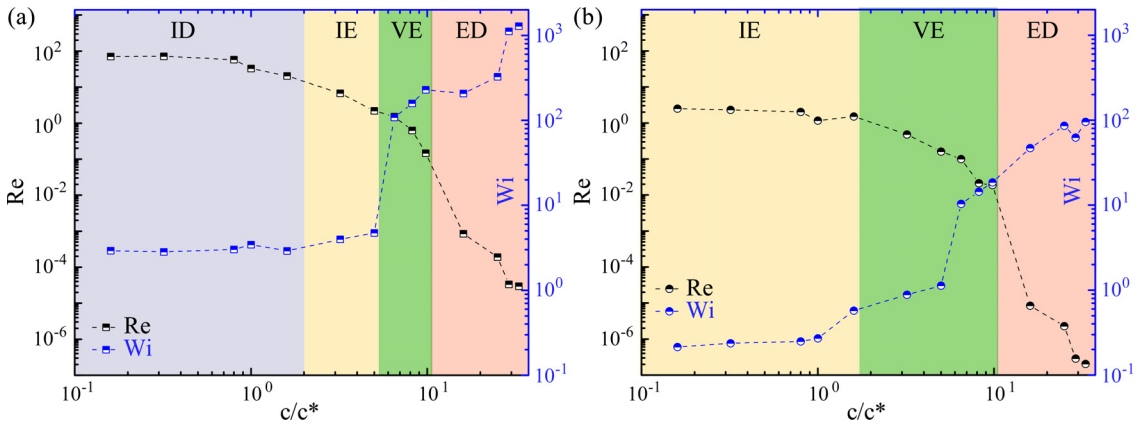

FIG. 5. Variation of Reynolds number *Re* and Weissenberg number *Wi* with c/c^* for (a) VFM and (b) DSM. (Note: ID: inertia dominated; IE: inertio-elastic; VE: viscoelastic; ED: elasticity dominated.

are comparable with the elastic forces for $c/c^* < 1.6$ and become trivial beyond that. As a result, the flow dynamics is inertia dominated in VFM, whereas it is inertio-elastic in DSM for $c/c^* < 1.6$. Consequently, the elastic forces in VFM cannot surpass the strong inertial forces, and the effect of polymer remains quiescent. On the other hand, the weak presence of inertial forces in this regime for DSM coupled with spreading induced polymeric chain elongation causes a reduction in the exponent of growth of the bridge height. Thus, VFM is inherently associated with stronger inertial forces, which results in higher exponent of growth in the absence or presence of weak elastic forces. This also explains why Sellier *et al.*[43] observed a faster neck growth for the volume growth method as compared to spreading for Newtonian fluid. However, at sufficiently large polymer concentrations ($c/c^* > 9.8$), the polymer chains get highly entangled, and a notable effect of elasticity is observed. It is also evident from the above discussion that the thin film equation can only be applied for $c/c^* \geq 9.8$, where the effect of inertial forces is less.

We suggest that similar to Newtonian fluids, early stages of coalescence of polymeric drops can also be characterized by a self-similar meniscus profile. However, a scaling parameter same as that of Newtonian fluids cannot be chosen due to the presence of an inherent relaxation time scale in the polymeric fluids. In fact, Varma *et al.*[35] showed that the relaxation time scale, λ, is the most important nodal parameter that governs the power law behavior of the polymeric liquid. Hence, the self-similar parameter is perturbed with the Weissenberg number, *Wi*, to accommodate the inherent time scale of polymers into the similarity parameter. The new self-similar regime for polymeric coalescence is expressed as

$$h(x,t) = h_b(t)\zeta(\xi), \quad \xi = \frac{\theta x}{2vt}\left(1 + \frac{1}{1+Wi}\right), \tag{2}$$

where $h(x, t)$ is the droplet shape, h_b is the instantaneous height of the bridge, $\zeta(\xi) = h(x,t)/h_b$ is the similarity profile of the bridge, ξ is the similarity variable, and v is the velocity of bridge. Substitution of $Wi = 0$ in Eq. (2) reduces the similarity variable to $\xi = \frac{\theta x}{vt}$, which is the similarity parameter adopted by Hernández-Sánchez *et al.*[19] for Newtonian fluid. The raw data depicting the temporal evolution of the bridge profile for $c/c^* = 0.32$ and 1.6 along with the bridge profiles after re-scaling with the similarity parameter have been presented in Figs. S1(a) and S1(b), respectively. The collapse of data suggests that similar to Newtonian fluid, polymeric droplets also display self-similarity at early stages of coalescence.

We finally attempt to describe the self-similar bridge profile using the thin film lubrication model. In this regard, we appeal to Varma *et al.*,[35] who applied the linear Phan-Thein–Tanner (PTT)[50,51] constitutive relation to obtain a modified thin film lubrication equation without gravitational body force for polymeric droplets, in which κ is the model parameter of linear PTT, η_o is the zero shear viscosity of the fluid, λ is the relaxation time, and σ is the surface tension of the fluid,

$$\frac{\partial h}{\partial t} + \frac{\sigma}{3\eta_o}\frac{\partial}{\partial x}\left[h^3\frac{\partial^3 h}{\partial x^3} + \frac{6\kappa\lambda^2\sigma^2}{5\eta_o^2}h^5\left(\frac{\partial^3 h}{\partial x^3}\right)^3\right] = 0. \tag{3}$$

Substituting the similarity parameter into Eq. (3) leads to an ordinary differential equation for the similarity profile $\zeta(\xi)$, given as

$$\zeta - \xi\zeta' + \frac{\left(1+\frac{1}{1+Wi}\right)^4}{16V}\left(\zeta^3\zeta'''\right)' + \frac{27\kappa Wi^2}{2560\theta^2V^3}\left(1+\frac{1}{1+Wi}\right)^{10}\left(\zeta^5(\zeta''')^3\right)' = 0. \tag{4}$$

Here, $V = 0.818\,809$ is a numerical constant for Newtonian fluid[19] obtained by scaling the coalescence velocity, v, such that

$$v = V\frac{\sigma}{3\eta_o}\theta^4. \tag{5}$$

For Newtonian fluid, $Wi = 0$, and Eq. (4) reduces to the one proposed by Hernandez *et al.*[19] Next, we list down the boundary conditions required to solve Eq. (4). As the two droplets are symmetric at $x = 0$,

$$\zeta(0) = 1, \quad \zeta'(0) = 0, \quad \zeta'''(0) = 0. \tag{6}$$

The far away bridge profile should match the slope of the contact angle θ. Hence, the far away boundary condition is expressed as

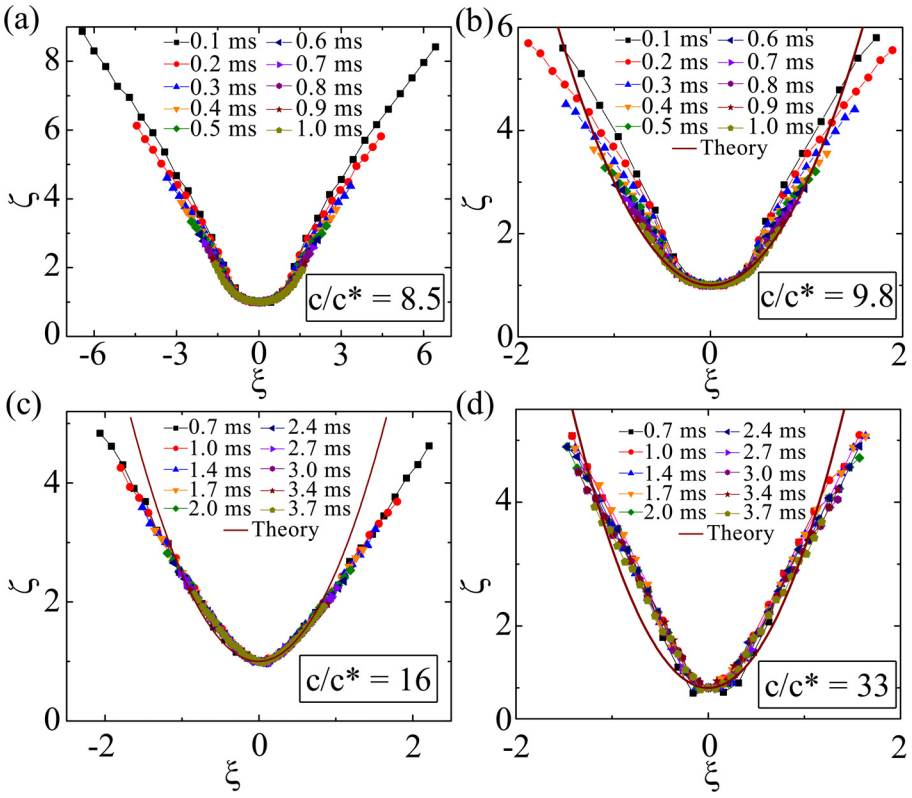

FIG. 6. (a)–(d) The re-scaled bridge profile for $c/c^* = 8.5$, 9.8, 16, and 33 at different time instants and a self-similar dynamics through the collapse of data. The solid red line represents predicted theoretical profile.

$$\zeta''(\infty) = 0. \tag{7}$$

Figures 6(a)–6(d) show the bridge profile for $c/c^* = 8.5$, 9.8, 16, and 33 at different instants of time, respectively. The raw data for the corresponding concentration ratios are given in Figs. S2(a)–S2(d). As our previous discussion on predominant forces has already established that the thin film approximation is only applicable for the semi dilute entanglement regime, the theoretical profile (solid line) obtained from the lubrication model is shown for $c/c^* = 9.8$, 16, and 33 given in Figs. 6(b)–6(d). Convincing agreement between the experimental and theoretical profiles suggests that the lubrication model is capable of predicting the coalescence dynamics to an acceptable level. However, some deviation between the experimental and theoretical profiles can be observed, which may have resulted due to pinning[52] on the needle surface or the continuous volume growth of the droplets.

V. CONCLUSION

We unveil that the two methods of merging of droplets, namely, the volume filling method (VFM) and the droplet spreading method (DSM), lead to dramatically different coalescence dynamics of complex rheology fluids due to their interaction with the solid–liquid interface. A discussion on non-dimensional numbers (*Re*, *Wi*) suggests that VFM is inherently associated with strong inertial forces. Moreover, unlike DSM that induces polymer chain elongation, the polymer chains in VFM remain at a relaxed state due to continuous fluid pumping. Consequently, the influence of polymer on the bridge evolution remains quiescent until the polymer chains get highly entangled at large polymer concentrations ($c/c^* > 9.8$). The bridge profiles when rescaled with a similarity parameter that incorporates the effect of relaxation time scale display a self-similar dynamics. Employing the similarity solution in a modified thin film equation for polymers also demonstrates a universal shape of the bridge for $c/c^* \geq 9.8$. However, incorporating the effect of volume growth on polymer chains in the theoretical model can provide better agreement with experimental results and warrants future investigation. The present findings provide a road map for potential innovations in industrial applications tuned for volume growth coalescence of polymeric droplets.

SUPPLEMENTARY MATERIAL

See the supplementary material for the bridge profiles during coalescence.

ACKNOWLEDGMENTS

A.K. acknowledges partial support from the office of the Principal Scientific Adviser to the Government of India.

AUTHOR DECLARATIONS

Conflict of Interest

The authors have no conflicts to disclose.

Author Contributions

Sarath Chandra Varma: Conceptualization (equal); Data curation (equal); Formal analysis (equal); Investigation (lead); Methodology

(equal); Validation (equal); Writing – original draft (equal); Writing – review & editing (equal). **Debayan Dasgupta:** Data curation (equal); Formal analysis (equal); Investigation (supporting); Validation (equal); Writing – original draft (equal). **Aloke Kumar:** Conceptualization (lead); Formal analysis (equal); Funding acquisition (lead); Methodology (equal); Project administration (lead); Resources (lead); Supervision (lead); Writing – review & editing (equal).

DATA AVAILABILITY

The data that support the findings of this study are available within the article and its supplementary material.

REFERENCES

[1]M. Wu, T. Cubaud, and C.-M. Ho, "Scaling law in liquid drop coalescence driven by surface tension," Phys. Fluids **16**, L51–L54 (2004).
[2]N. Ashgriz, *Handbook of Atomization and Sprays: Theory and Applications* (Springer Science & Business Media, 2011).
[3]X. Gao, H. Chen, Q. Nie, and H. Fang, "Stability of line shapes in inkjet printing at low substrate speeds," Phys. Fluids **34**, 032002 (2022).
[4]H. Sirringhaus, T. Kawase, R. Friend, T. Shimoda, M. Inbasekaran, W. Wu, and E. Woo, "High-resolution inkjet printing of all-polymer transistor circuits," Science **290**, 2123–2126 (2000).
[5]Y. Zhang, Y. Chen, P. Li, and A. T. Male, "Weld deposition-based rapid prototyping: A preliminary study," J. Mater. Process. Technol. **135**, 347–357 (2003).
[6]P. J. Graham, M. M. Farhangi, and A. Dolatabadi, "Dynamics of droplet coalescence in response to increasing hydrophobicity," Phys. Fluids **24**, 112105 (2012).
[7]Y. Nam, D. Seo, C. Lee, and S. Shin, "Droplet coalescence on water repellant surfaces," Soft Matter **11**, 154–160 (2015).
[8]F. Chu, X. Wu, Y. Zhu, and Z. Yuan, "Relationship between condensed droplet coalescence and surface wettability," Int. J. Heat Mass Transfer **111**, 836–841 (2017).
[9]F. Y. Leong and D.-V. Le, "Droplet dynamics on viscoelastic soft substrate: Toward coalescence control," Phys. Fluids **32**, 062102 (2020).
[10]M. W. Lee, N. Y. Kim, S. Chandra, and S. S. Yoon, "Coalescence of sessile droplets of varying viscosities for line printing," Int. J. Multiphase Flow **56**, 138–148 (2013).
[11]V. Kulkarni, V. Y. Lolla, S. R. Tamvada, N. Shirdade, and S. Anand, "Coalescence and spreading of drops on liquid pools," J. Colloid Interface Sci. **586**, 257–268 (2021).
[12]H. Deka, G. Biswas, S. Chakraborty, and A. Dalal, "Coalescence dynamics of unequal size drops," Phys. Fluids **31**, 012105 (2019).
[13]A. S. Hsu, A. Roy, and L. G. Leal, "Drop-size effects on coalescence of two equal-sized drops in a head-on collision," J. Rheol. **52**, 1291–1310 (2008).
[14]M. A. Nilsson and J. P. Rothstein, "The effect of contact angle hysteresis on droplet coalescence and mixing," J. Colloid Interface Sci. **363**, 646–654 (2011).
[15]J. Z. Chen, S. M. Troian, A. A. Darhuber, and S. Wagner, "Effect of contact angle hysteresis on thermocapillary droplet actuation," J. Appl. Phys. **97**, 014906 (2005).
[16]R. Narhe, D. Beysens, and Y. Pomeau, "Dynamic drying in the early-stage coalescence of droplets sitting on a plate," Europhys. Lett. **81**, 46002 (2008).
[17]W. D. Ristenpart, P. M. McCalla, R. V. Roy, and H. A. Stone, "Coalescence of spreading droplets on a wettable substrate," Phys. Rev. Lett. **97**, 064501 (2006).
[18]M. W. Lee, D. K. Kang, S. S. Yoon, and A. L. Yarin, "Coalescence of two drops on partially wettable substrates," Langmuir **28**, 3791–3798 (2012).
[19]J. F. Hernández-Sánchez, L. A. Lubbers, A. Eddi, and J. H. Snoeijer, "Symmetric and asymmetric coalescence of drops on a substrate," Phys. Rev. Lett. **109**, 184502 (2012).
[20]Y. Sui, M. Maglio, P. D. Spelt, D. Legendre, and H. Ding, "Inertial coalescence of droplets on a partially wetting substrate," Phys. Fluids **25**, 101701 (2013).
[21]A. Eddi, K. G. Winkels, and J. H. Snoeijer, "Influence of droplet geometry on the coalescence of low viscosity drops," Phys. Rev. Lett. **111**, 144502 (2013).
[22]N. D. Pawar, S. S. Bahga, S. R. Kale, and S. Kondaraju, "Symmetric and asymmetric coalescence of droplets on a solid surface in the inertia-dominated regime," Phys. Fluids **31**, 092106 (2019).
[23]M. van Dongen, A. van Loon, R. Vrancken, J. Bernards, and J. Dijksman, "UV-mediated coalescence and mixing of inkjet printed drops," Exp. Fluids **55**, 1744 (2014).
[24]A. Klestova, E. Sergeeva, and A. V. Vinogradov, "Inkjet printing in liquid media: Intra-volumetric drop coalescence in polymers," Coatings **9**, 275 (2019).
[25]A. B. Pawar, M. Caggioni, R. Ergun, R. W. Hartel, and P. T. Spicer, "Arrested coalescence in pickering emulsions," Soft Matter **7**, 7710–7716 (2011).
[26]C. P. Whitby and M. Krebsz, "Coalescence in concentrated pickering emulsions under shear," Soft Matter **10**, 4848–4854 (2014).
[27]S. Goel and A. Ramachandran, "The suppression of droplet-droplet coalescence in a sheared yield stress fluid," J. Colloid Interface Sci. **492**, 199–206 (2017).
[28]T. Krebs, K. Schroën, and R. Boom, "Coalescence dynamics of surfactant-stabilized emulsions studied with microfluidics," Soft Matter **8**, 10650–10657 (2012).
[29]S. C. Varma, A. Saha, S. Mukherjee, A. Bandopadhyay, A. Kumar, and S. Chakraborty, "Universality in coalescence of polymeric fluids," Soft Matter **16**, 10921–10927 (2020).
[30]J. D. Paulsen, J. C. Burton, and S. R. Nagel, "Viscous to inertial crossover in liquid drop coalescence," Phys. Rev. Lett. **106**, 114501 (2011).
[31]X. Xia, C. He, and P. Zhang, "Universality in the viscous-to-inertial coalescence of liquid droplets," Proc. Natl. Acad. Sci. **116**, 23467–23472 (2019).
[32]M. M. Rahman, W. Lee, A. Iyer, and S. J. Williams, "Viscous resistance in drop coalescence," Phys. Fluids **31**, 012104 (2019).
[33]S. C. Varma, A. S. Rajput, and A. Kumar, "Rheocoalescence: Relaxation time through coalescence of droplets," Macromolecules **55**, 6031–6039 (2022).
[34]S. Chen, E. Pirhadi, and X. Yong, "Viscoelastic necking dynamics between attractive microgels," J. Colloid Interface Sci. **618**, 283–289 (2022).
[35]S. C. Varma, A. Saha, and A. Kumar, "Coalescence of polymeric sessile drops on a partially wettable substrate," Phys. Fluids **33**, 123101 (2021).
[36]H. Chen, X. Pan, Q. Nie, Q. Ma, H. Fang, and Z. Yin, "Probing the coalescence of non-Newtonian droplets on a substrate," Phys. Fluids **34**, 032109 (2022).
[37]P. J. Dekker, M. A. Hack, W. Tewes, C. Datt, A. Bouillant, and J. H. Snoeijer, "When elasticity affects drop coalescence," Phys. Rev. Lett. **128**, 028004 (2022).
[38]M. A. Fardin, M. Hautefeuille, and V. Sharma, "Spreading, pinching, and coalescence: The Ohnesorge units," Soft Matter **18**, 3291–3303 (2022).
[39]C. Clasen, J. Eggers, M. A. Fontelos, J. Li, and G. H. McKinley, "The beads-on-string structure of viscoelastic threads," J. Fluid Mech. **556**, 283–308 (2006).
[40]J. Eggers, M. A. Herrada, and J. Snoeijer, "Self-similar breakup of polymeric threads as described by the Oldroyd-B model," J. Fluid Mech. **887**, A19 (2020).
[41]P. C. Duineveld, "The stability of ink-jet printed lines of liquid with zero receding contact angle on a homogeneous substrate," J. Fluid Mech. **477**, 175–200 (2003).
[42]P. M. Somwanshi, K. Muralidhar, and S. Khandekar, "Dropwise condensation patterns of bismuth formed on horizontal and vertical surfaces," Int. J. Heat Mass Transfer **122**, 1024–1039 (2018).
[43]M. Sellier and E. Trelluyer, "Modeling the coalescence of sessile droplets," Biomicrofluidics **3**, 022412 (2009).
[44]O. Arnolds, H. Buggisch, D. Sachsenheimer, and N. Willenbacher, "Capillary breakup extensional rheometry (CaBER) on semi-dilute and concentrated polyethyleneoxide (PEO) solutions," Rheol. Acta **49**, 1207–1217 (2010).
[45]V. Tirtaatmadja, G. H. McKinley, and J. J. Cooper-White, "Drop formation and breakup of low viscosity elastic fluids: Effects of molecular weight and concentration," Phys. Fluids **18**, 043101 (2006).
[46]R. B. Bird, R. C. Armstrong, and O. Hassager, *Dynamics of Polymeric Liquids, Volume 1: Fluid Mechanics* (John Wiley and Sons Inc., New York, 1987).
[47]M. Rubinstein and R. H. Colby *et al.*, *Polymer Physics* (Oxford University Press, New York, 2003), Vol. 23.
[48]Y. Liu, Y. Jun, and V. Steinberg, "Concentration dependence of the longest relaxation times of dilute and semi-dilute polymer solutions," J. Rheol. **53**, 1069–1085 (2009).

[49]F. Del Giudice, G. D'Avino, F. Greco, I. De Santo, P. A. Netti, and P. L. Maffettone, "Rheometry-on-a-chip: Measuring the relaxation time of a viscoelastic liquid through particle migration in microchannel flows," Lab Chip **15**, 783–792 (2015).
[50]N. Phan-Thien, "A nonlinear network viscoelastic model," J. Rheol. **22**, 259–283 (1978).
[51]S.-C. Xue, R. Tanner, and N. Phan-Thien, "Numerical modelling of transient viscoelastic flows," J. Non-Newtonian Fluid Mech. **123**, 33–58 (2004).
[52]N. K. Chandra, U. U. Ghosh, A. Saha, and A. Kumar, "Contact line pinning and depinning can modulate the rod-climbing effect," Langmuir **37**, 14785–14792 (2021).